Dynamics of towed particles in a turbulent flow

M. Obligado, Mickaël Bourgoin

Dynamics of towed particles in a turbulent flow

M. Obligado

Univ. Grenoble Alpes, CNRS, Grenoble INP, LEGI, 38000 Grenoble, France*

M. Bourgoin

Laboratoire de Physique de l'École Normale Supérieure de Lyon, CNRS & Université de Lyon, 46 allée d'Italie, F-69364 Lyon Cedex 07, France

Abstract

We present an experimental study exploring the dynamics of inertial spheres towed at a constant mean velocity in a turbulent flow. Our work focuses on finite size particles, in the sense that their diameter is significantly larger than the dissipation scale and lies in the range of inertial scales of the background turbulence. Our experimental setup allows to register the Lagrangian velocity and acceleration of particles with different diameters, densities and free-stream velocities. The analysis of towed particles dynamics shows a clear trend of velocity and acceleration fluctuations to be reduced with increasing particle inertia, while acceleration fluctuations are found to be Gaussian, at odds of usual results for finite-size freely advected particles. Besides, the multi-scale spectral dynamics of the particle is shown to be related to that of the background turbulence by a linear second-order band-pass transfer function. We analyse this behaviour at the light of a simple model where the coupling between the particle and the flow is entirely attributed to the drag force, a usual approach for dense point-like particles freely-advected in a turbulent flow, which is known however to fail predicting the transport of freely advected finite-size particles. We show that this drag-dominated model quantitatively predicts the dynamics of finite size towed particles, simply requiring to tune the effective particle response time. This suggests that, contrary to the case freely advected finite size inertial particles, the towing configuration efficiently emphasizes the actual role of the drag force by imposing it as an unambiguous leading term in towed particle / turbulence interactions.

Keywords: Particle-laden turbulent flows, towed systems, Lagrangian analysis

1. Introduction

Flows transporting particles are ubiquitous in natural and human-made systems. The study of material inclusions interacting with a turbulent carrier flow is a deep fundamental problem that requires understanding of the coupling between particles and a multi-scale turbulent flow. From a quantitative point of view, no general model to describe and accurately predict the statistical properties of all sort of inclusions advected by a turbulent flow has emerged yet. The most reliable model available relies on the Maxey-Riley-Gatignol equation [1, 2], that extends the Basset-Boussinesq-Oseen-Tchen equation [3] to the case of unsteady non-uniform flow. This equation applies to the case of particle Reynolds number and particle shear number smaller that one. Such point-like particle scenario is usually related to particles smaller than the smallest dissipative structures of the carrier turbulent flow, characterised by the dissipation scale (also called the Kolmogorov scale) $\eta = \left(\nu^3/\varepsilon\right)^{1/4}$, with ν the kinematic viscosity of the fluid and ε the turbulent energy dissipation rate per unit of mass. First order corrections (known as Faxén corrections) have been proposed, to account for local variations of the flow properties at the scale of the particles, although they have been shown to be insufficient for particles larger than a few dissipative scales [4]. For the case of heavy point particles, a common simplification used in most theoretical and numerical studies [5], assumes that the dynamics of the particles is solely controlled by the Stokes drag force, in which case the particle equation of motion simply becomes

$$\frac{\mathrm{d}\vec{v}}{\mathrm{d}t} = \frac{1}{\tau_p}(\vec{u} - \vec{v}), \tag{1}$$

where τ_p is the particle's viscous response time, $\vec{v}$ is the particle's velocity vector and $\vec{u}$ is the fluid's velocity at the position of the particle. Within this simplification, the coupling between particles inertia and turbulence is quantified by the Stokes number $St = \tau_p/\tau_\eta$, with $\tau_\eta = (\nu/\varepsilon)^{1/2}$ the turbulent dissipation time scale. As a first approximation (neglecting, for instance, the eventual preferential sampling of specific regions of the flow by the particles) equation (1) can be interpreted as a first order low-pass

filter with a characteristic filtering time τ_p, where the velocity $\vec{v}$ of the inertial particle is mainly given by the filtered velocity of the fluid $\vec{u}$ [6]. This shall result, in particular, in a decrease of particles velocity and acceleration fluctuations with increasing Stokes number. This simplified description of the turbulent dynamics of inertial particles seems to be accurate, to some extent, for sub-Kolmogorov particles. For instance the trend of acceleration statistics to become less intermittent as the Stokes number increases [7] has been qualitatively confirmed in wind-tunnel experiments investigating the Lagrangian dynamics of small water droplets [8].

The coupling between small particles and turbulence is further affected when particles are subject to an important mean drift. It has been shown, for instance, that the drift induced by gravity have drastic effects even on the dynamics of microbubbles with very small Stokes number [9]. Similarly, the impact of gravitational drift on Stokes number filtering effects associated to eq. (1) has been rationalised by Csanady [10] who showed that settling particles tend to have increased fluctuations due to the enhanced decorrelation of their dynamics as they cross turbulent eddies while they settle (*crossing trajectory effect*). A similar role due to drift can also emerge when particles are towed in a turbulent medium. This arises for instance for towed or self-propelled instrumentation [11, 12], a problem which has been recently revisited by Calzavarini and co-workers [13] who performed numerical simulations of inertia-less particles towed in homogeneous isotropic turbulence.

The present study aims at exploring experimentally the dynamics of inertial spheres towed at constant mean velocity in a turbulent flow. In regard to practical applications, the considered spheres are finite sized, in the sense that their diameter is significantly larger than the dissipation scale η of the background turbulence.

This is a follow up of a previous preliminary work [14] where we characterized velocity and acceleration statistics of towed spheres with different diameters and densities at a fixed towing velocity of approximately 10 m/s. As in the present work the background flow was grid-generated turbulence, with good levels of homogeneity and isotropy. The novelty of the present work is twofold. First, we expand previous results by exploring different freestream velocities. We also develop a theoretical model that allows to study this system in higher depth with a relevant framework to connect the

fluctuating dynamics of the towed particles (parametrized by a modified Stokes time) to that of the background turbulence.

In both, the previous and present, studies the towing configuration is artificially obtained by considering a steady thin cable (with one fix end and a free tip end to which a sphere is attached) in a horizontal wind-tunnel. This reproduces the situation of an object towed horizontally at constant speed. This configuration is of interest as it also mimics the dynamics of towed and/or propelled particles. These systems are of practical interest not only in aeronautics, but also on the modelling of sensors [13], active [15, 16] and smart [17] particles.

From the particle-turbulence interaction point of view, the investigated situation of an attached sphere in a turbulent flow with a steady stream $<\vec{U}>=U_z\vec{e}_z$ (with e_z the streamwise direction of the wind tunnel) can also be considered as a a semi-constrained inclusion (its motion is constrained to remain in the xy plane) interacting with a surrounding turbulent flow, where the role of drag can be expected to play a predominant role (due to the strong drift velocity respect to the main stream) as in the classical inertial point-particle model in equation (1), although with possible non-linear drag effects, leading to a particle response time τ_p eventually dependent on the particles towing velocity via finite particles' Reynolds number effects.

In our previous study [14], we considered the influence of particles inertia on its velocity and acceleration Lagrangian statistics and energy spectral density. Results suggested a band-pass filtering scenario (particles dynamics being reasonably retrieved from the carrier flow turbulent fluctuations by a band-pass filter). The low-pass contribution to this filtering was consistent with a drag-dominated coupling of the form of (1). The low-pass frequency cut-off is then expected to be related to particle's inertia and its viscous relaxation τ_p. The high-pass part of the band-pass filtering, was attributed to the cable's effect, which limits the large-scale motion of the system. Nevertheless, in spite of these reasonable qualitative interpretations, many questions remained unanswered. In particular, no systematic study was performed on the dynamics of the towed spheres for different streamwise velocities and no physical modeling was given for the band-pass filtering scenario, allowing to quantitatively relate particles fluctuating dynamics to that of the background turbulence.

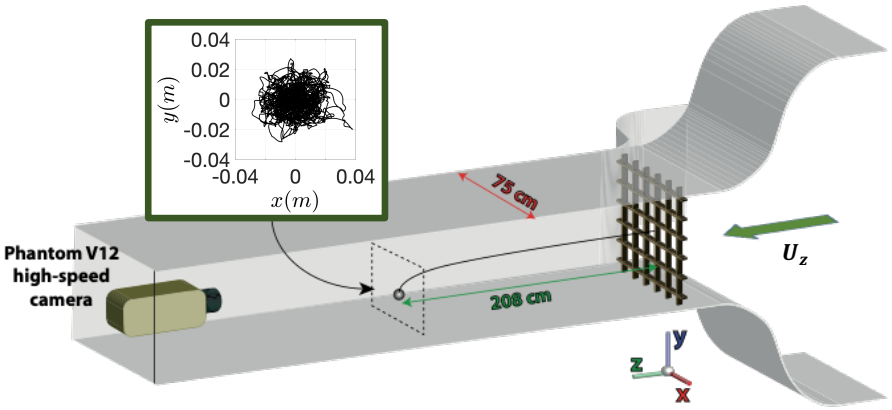

Figure 1: Schema of the experimental setup. The measurement plane is located 2.08m downstream the grid, in a region where the turbulence is fully developed, homogeneous and isotropic.

This is the goal of the present study. While we explore here the same range of diameters and densities than in [14], three different freestream velocities ($\sim$ 7.3, 9.9 and 12.4 m/s) are now tested. We also cover a large range of particle Reynolds numbers (defined as $Re_p = U_z d_p/\nu$, with d_p the particles' diameter and $\nu \approx 1.5 \times 10^{-5}\mathrm{m}^2/\mathrm{s}$ the kinematic velocity of air at operating conditions), of $Re_p \in [800, 5000]$. This allows us to confirm the previously suggested band-pass scenario for a wider parameter space, and to propose a simple model for the underlying particle-turbulence coupling. The characteristic frequencies of the filter are found to be dependent on the tension of the cable, the particle viscous response time and the freestream velocity. Despite the simplifications used for the modeling, such as ignoring the complex dynamics of the cable and the added mass term, experimental observations are in reasonable quantitative agreement with the model.

2. Experimental setup

The experiment has been run in the 'Lespinard' large wind tunnel in LEGI laboratory. It is a closed-circuit wind tunnel with a measurement section of 0.75 m$\times$0.75 m$\times$4 m (figure 1). Turbulence is generated with a passive grid, which produces a background flow with a turbulence intensity $\sigma_{u_z}/U_z \simeq 3\%$. In the following we will refer to the

total streamwise velocity as $u_z = U_z + \tilde{u}_z$ with U_z the mean streamwise velocity and $\tilde{u}_z$ its fluctuating part, which has a standard deviation value σ_{u_z}. We performed experiments at three different mean stream velocities $U_{z1} = (7.33 \pm 0.11)$ m/s, $U_{z2} = (9.89 \pm 0.08)$ m/s and $U_{z3} = (12.44 \pm 0.07)$ m/s, corresponding to different turbulent conditions. The main turbulence parameters induced in the tunnel for these velocities are shown in the table 1 (these values have been calculated using the results from previous studies on the same wind tunnel via hot-wire anemometry [18]).

	U_{z1}	U_{z2}	U_{z3}
η (μm)	320	260	220
Re_λ	125	146	164
λ (mm)	6.4	5.5	4.9
ε (m^2/s^3)	0.31	0.77	1.54
τ_η (ms)	6.9	4.4	3.1
T_e (s)	0.18	0.13	0.11

Table 1: Turbulence parameters for the velocities used. The parameter η is the Kolmogorov length scale and τ_η its associated time scale, λ the Taylor microscale and Re_λ its associated Reynolds number (defined as $Re_\lambda = \lambda \sigma_{u_z}/\nu$). ε is the turbulence dissipation rate and T_e is the Eulerian correlation time.

The cable used to tow the sphere is 2.08 m long and is composed of three filaments of Polyamide-Nylon with a diameter of 25 μm each and a maximum lineal density of 20 μg/cm. One of the cables extremity is attached to the grid, while a particle is attached at the other end. As a consequence, the particle's streamwise motion is blocked in the z direction, but the particle is free to move in the transverse directions x and y. It is this transverse dynamics that we record and analyse using high-speed imaging. We have previously addressed the relevance of the elasticity of the wire in a similar system [19], and it was found to be only significant in the large frequency range in the trajectories' spectral dynamics.

Seven different spheres were used in the experiment and they were all measured with the three different velocities. The parameters of the spheres are shown in table table 2. Table 3 contains the values of particle Reynolds numbers $Re_p = U_z d_p/\nu$, and

the particle viscous response time,

$$\tau_p = \frac{8m_p}{\pi d_p \mu_f Re_p C_D(Re_p)}, \tag{2}$$

with m_p the mass of the particle and μ_f the dynamic viscosity of air. The drag coefficient C_D is estimated according to the fit from Brown & Lawler [20],

$$C_D = \frac{24}{Rep}(1+0.150Re_p^{0.681}) + \frac{0.407}{1+\frac{8.710}{Re_p}}, \tag{3}$$

which is valid for for particles with Re_p up to 2×10^5. Table 3 also shows the value of St (defined as $St = \tau_p/\tau_\eta$) and an alternative definition of the Stokes number, $St_D = \tau_p/\tau_D$ with $\tau_D = \frac{d_p^{2/3}}{\varepsilon^{1/3}}$ is the characteristic time of turbulence at the scale of the particle. St and St_D are simply related by $St_D = St \times \left(\frac{\eta}{d_p}\right)^{2/3}$.

Sphere	Weight (mg)	Diameter (mm)	Density (kg/m^3)	$\delta_{density}$ (kg/m^3)
1	0.96	4.3	23.06	0.40
2	1.83	6.29	14.04	0.14
3	0.44	3.05	29.62	0.96
4	0.31	2.08	65.8	3.1
5	17.39	3.11	1104	11
6	14.29	1.79	4758	83
7	24.03	1.69	9510	173

Table 2: Weight, diameter and density of the spheres used in this work.

Particle trajectories in the plane xy were recorded with a high-speed camera Phantom V12 from Vision Research Inc. The camera was located inside the tunnel, at least 1 m downstream the particle to not affect its motion. Images were acquired at a frame rate of 3000 fps (see inset in figure 1). Each video lasts 6.15 s, what corresponds to at least ~ 34 integral time scales of the carrier flow. For each class of particles and each free stream velocity, we record typically 40 videos, what corresponds to a total recording time of more than 1.3×10^3 integral time scales of the carrier flow. As all studied particles are macroscopic (their image covers at least several hundreds of

Sphere	$Re_p(U_{z1})$	$Re_p(U_{z2})$	$Re_p(U_{z3})$	$\tau_p(U_{z1})(s)$	$\tau_p(U_{z2})(s)$	$\tau_p(U_{z3})(s)$	$St(U_{z1})$	$St(U_{z2})$	$St(U_{z3})$	$St_D(U_{z1})$	$St_D(U_{z2})$	$St_D(U_{z3})$
1	2101	2835	3566	0.039	0.030	0.024	5.652	6.818	7.742	0.9693	0.9733	0.9757
2	3074	4147	5217	0.036	0.027	0.021	5.217	6.136	6.774	0.7025	0.6907	0.6823
3	1490	2011	2530	0.033	0.026	0.021	4.783	5.909	6.774	1.049	1.073	1.092
4	1016	1371	1725	0.046	0.036	0.030	6.667	8.182	9.677	1.870	1.952	2.018
5	1520	2051	2579	1.248	0.966	0.782	180.9	219.5	252.3	38.69	39.56	40.23
6	875	1180	1485	2.738	2.178	1.804	396.8	495.0	581.9	122.6	128.9	134.0
7	826	1114	1402	5.087	4.057	3.366	737.2	922.0	1086	236.8	249.5	260.0

Table 3: Particle Reynolds number, particle viscous time, St and St_D for each sphere and flow Reynolds number.

pixels), standard image processing techniques allowed us to detect their centers with sub-pixel accuracy (a typical trajectory can be observed in the inset in figure 1). Each image contains a single particle, and its position is efficiently determined frame by frame with sub-pixel accuracy with a center of mass analysis. The conversion from pixels to length units is previously calibrated using a known printed patron (mask) which allows to determine the projective transformation between pixels and real world units. The pixel size recorded by the camera slightly changes between experiments but it stayed close to 180 μm. In our experimental conditions, this rationale allowed us to achieve a sub-pixel resolution of 55 μm in the two components of the particle centre vector.

Finally, particles velocity and acceleration are deduced from the trajectories via the spectral analysis proposed in [14]. It consists in removing the noise at high frequencies on the Lagrangian spectra, by modelling these range of frequencies with a power law. This method allows to produce the probability density functions (PDFs) of both Lagrangian velocity and acceleration.

In order to explore the aforementioned filtering scenario connecting particle and turbulence dynamics, spectral analysis of the particle trajectories is used in conjunction with the spectra of the carrier flow obtained from hot-wire anemometry. This allows to define the spectral transfer function,

$$H^2 = \frac{\|\widehat{v}\|^2}{\|\widehat{u}\|^2}, \tag{4}$$

where $\|\widehat{v}\|$ is the particle Lagrangian velocity's power spectral density and $\|\widehat{u}\|$ is the

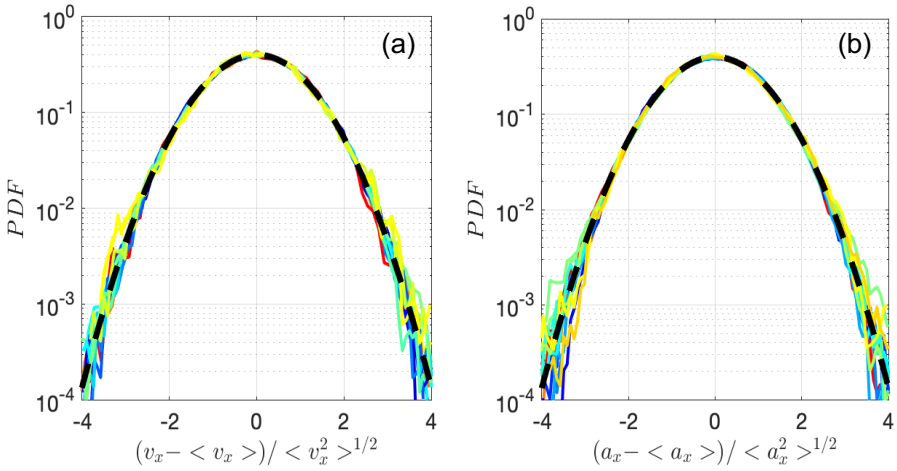

Figure 2: Probability density functions (centered and normalised to variance one) of the horizontal velocity (a) and acceleration (b) for all the particles investigated. The black dashed line, in the figures, is a Gaussian with variance 1.

temporal power spectral density of the background flow. The latter was measured in the plane of motion of the particle with a Dantec Dynamics 55P01 single hot-wire probe, made of a Pt-W wire with 5μm diameter, 3 mm long and a sensing length of 1.25 mm. Hot-wire signals were sampled at 3 kHz for at least 60s in constant temperature (CTA) mode.

3. Results

The PDFs of the horizontal velocity and acceleration for all datasets, centred and normalised by the variance, are presented in figure 2 (the vertical components u_y and a_y are not shown but present identical trends). It can be observed that all the PDFs collapse onto a Gaussian distribution. These results have been already observed in [14], but only for $U_{z2} = 9.89$m/s. While Gaussianity of velocity statistics is a standard result when studying particles in homogenous and isotropic turbulence, Gaussianization of acceleration has not been observed before on similar circumstances for freely advected finite size particles. For instance, experiments by Qureshi *et al.* [21] and Zimmermann *et*

al. [22] report that acceleration statistics remain robustly non-Gaussian even for finite-size inertial particles. This is in contradiction with predictions from the point-particle model (see equation (1)), which was shown numerically to promote the progressive Gaussianization of acceleration statistics as the Stokes number increases [7].

Contrary to freely advected finite size particles, the present results for the semi-constrained particle present a remarkable Gaussianity for acceleration. Interestingly, the dynamics of the towed particle has lost all evidence of intermittency from the surrounding turbulence. This Gaussianization of acceleration statistics recalls that observed numerically for the point-particle model reported previously [7], where particles with high inertia, and hence with large relative velocities ($\vec{u}-\vec{v}$) are found to have Gaussian acceleration statistics. The similarity with the present situation may be related to the important relative drift velocity of the towed sphere compared to the turbulent fluctuations (the difference being that for freely advected particles drift is intimately related to the particle response time τ_p, while for the towed particles drift velocity is set independently of τ_p). The low turbulence intensity of our experiment (imposing that the ratio of the fluctuating velocity to the mean drift velocity U_z is of the order of 3%) would avoid in the present case the possibility to explore intermediate situations (where the drift would be comparable to turbulent fluctuations) and hence to investigate the progressive Gaussianization process (all the cases we investigated are exactly Gaussian). It would be interesting in the future to investigate situations at higher turbulent intensity in order to explore the restitution of intermittency on the towed particle. This could be done by using active-grid turbulence and/or by gradually releasing the longitudinal motion of the towed particle, in order to span all situations from purely towed to freely advected particle. An interesting aspect of such a study would be to systematically vary the role of relative drift velocity on the Lagrangian intermittency of finite size particles in turbulence, independently of that of the response time of the particle.

As velocity and accelerations PDFs are Gaussian, they can be simply characterised by their standard deviation. Figure 3a shows the particle velocity turbulent intensity for the horizontal and vertical components of the velocity $\sigma_{v_{x,y}}/U$ as a function of particle Stokes number for all free stream velocities studied. First, we observe that veloc-

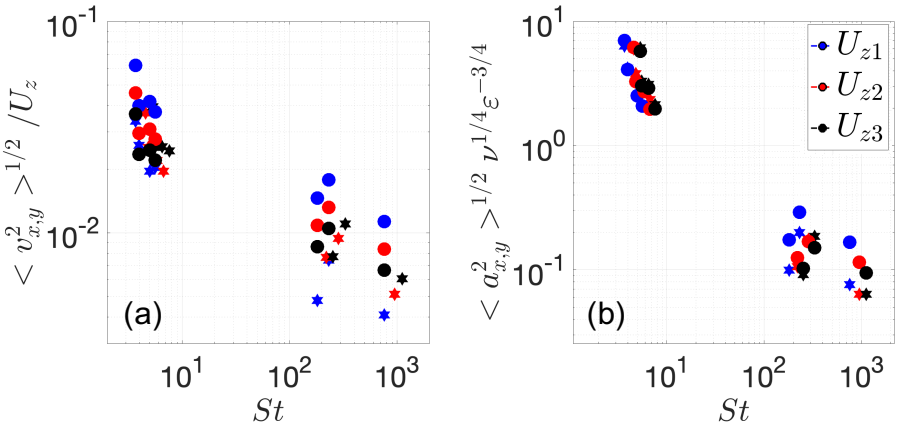

Figure 3: (a): Fluctuations of horizontal (stars) and vertical (circles) components of velocity. (b) Standard deviations of acceleration normalized with Heisenberg-Yaglom parameters for the horizontal and vertical components (same symbols as before).

ity relative fluctuations tend to globally decrease with particle's inertia, in qualitative agreement with a low-pass filtering effect due to particle inertia as usually predicted with drag dominated models in the spirit of the Tchen-Hinze theory [23]. A closer look at figure 3 shows a small anisotropy in particle's dynamics, evidenced by slightly larger fluctuations for the vertical component. It can also be observed that σ_{v_x}/U increases with the free stream velocity U_z, while the vertical component σ_{v_y}/U shows the opposite trend.

Figure 3b shows the standard deviation of both components of the acceleration normalized by the Heisenberg-Yaglom scaling (discussed in detail below) for the carrier turbulence acceleration variance, once more as a function of St. This parameter exhibits a similar trend than the standard deviation of velocity. In particular it is found to globally decrease with increasing inertia (a trend previously observed for the acceleration variance of finite-sized freely advected particles [21]). No particular trend is observed for acceleration variance with the free stream velocity. This suggests that the main forcing on the particle comes indeed from the turbulence and not from instabilities in the towing cable as reported in [19].

3.1. Transfer functions analysis

In this section we will first show how our results are compatible with a filtering scenario. As discussed before, this will be achieved via the transfer function H. Figure 4a shows two typical power spectral densities of particles velocities, at low and large inertia. From now on, we report results for the horizontal coordinate x of the particle trajectories, as in all cases the vertical one gives similar results.

Interestingly, all spectra collapse at low frequencies. Spectra in this low frequency regime follow a f^2 scaling, what can be related to the influence of the cable which constrains the motion of the particle to be bounded, imposing the average velocity of the particle (and hence the density of energy at vanishing frequency $f \to 0$) to be null. On the other hand, the low-pass cut-off strongly depends on the particle class, and it tends to decrease with increasing value of St. Also, at low inertia a plateau is observed at the intermediate frequencies of the power spectral density, and its extent tends to decrease as St increases.

Figure 4b shows two typical energy transfer functions $H^2 = \|\widehat{v}_x\|^2/\|\widehat{u}_x\|^2$, one for low inertia particles and the other for large inertia. While the shape of the transfer function is clearly different from a first-order low-pass filter, we find that the global shape is relatively well approximated by a second-order band-pass filter (dashed lines on the figure). This filter is characterised by the transfer function,

$$H^2 = \frac{1}{1+Q^2\left(\frac{f}{f_0}-\frac{f_0}{f}\right)^2}, \tag{5}$$

with Q the quality factor and f_0 the central frequency. The second order filter can be seen as a combination of a first order high-pass and a first order low-pass filter and can be equivalently characterised by the corresponding low-pass and high-pass cut-off frequencies, f_{lp} and f_{hp}, as $f_0 = \sqrt{f_{hp} f_{lp}}$ and $Q = f_0/(f_{lp} - f_{hp})$. Fits shown in figure 4b actually correspond to a three parameters fit, to cater for the non-normalised nature of our transfer functions: $H^2 = \frac{C}{1+Q^2\left(\frac{f}{f_0}-\frac{f_0}{f}\right)^2}$. Experimental fits therefore provide the parameters C, Q and f_0.

Figures 5a&b show the trends of the high-pass f_{hp} (red square) and low-pass f_{lp} (blue circles) cut-off frequencies with τ_p and St, respectively. The high-pass filter

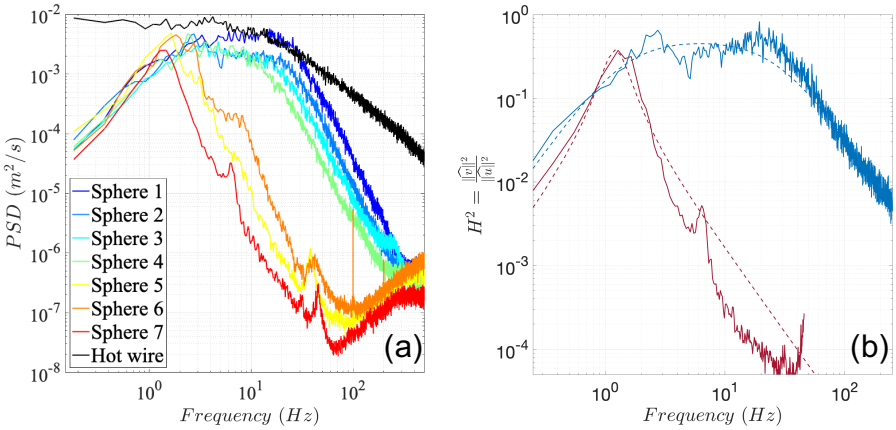

Figure 4: (a) Power spectral density of the velocity for all studied particles at U_{z3}. (b) Corresponding transfer functions for the second and the seventh particles. The dashed lines correspond to a fit following equation 5.

frequency remains approximately constant throughout our dataset. Furthermore, we observe that, as predicted by drag models such as (1), the low-pass frequency f_{lp} does decrease with increasing particle inertia. Nevertheless, low-pass frequencies for lighter particles (low values of St) and denser particles (large values of St), do not seem to align onto a single $f_{lp} \sim \tau_p^{-1}$ curve (nor onto $f_{lp} \sim St^{-1}$ or $f_{lp} \sim St_D^{-1}$, see black dashed lines in figures 5a-c). Therefore, while we find qualitative agreement between experimental results and the band-pass filtering scenario, further analysis is needed. On the next section we will discuss a simple model capable of predicting not only such filter but also the frequencies f_{lp} and f_{hp} in terms of parameters from the problem.

4. Advected sphere in turbulence: the role of filtering effects.

4.1. Dynamical model for the attached particles motion

As already discussed, minimal drag models in the spirit of (1) cannot be directly applied to the present system as the constraints imposed by the cable must be taken into account. We propose here a simple extension of such models to include the role of the cable tension. In this first study we assume the cable to be straight, which is indeed the case for the lightest particles (which are also the largest and the ones with the larger

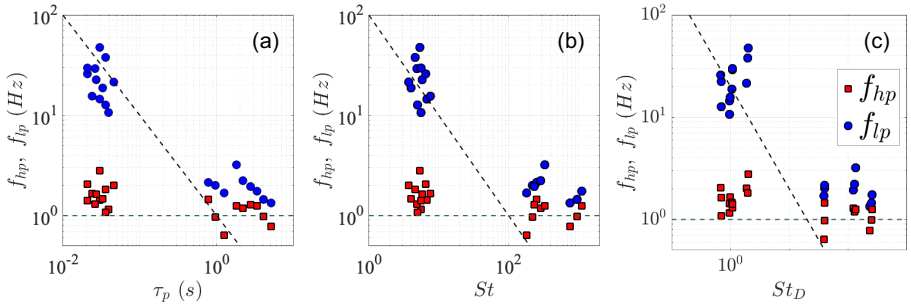

Figure 5: High-pass and low-pass frequencies obtained from the 2nd order band-pass model (equation 5) fit of the energy transfer function for all particles investigated, plotted as a function of the particle viscous response time (a), the Stokes number (b) and the corrected Stokes number St_D (c). In al cases the black dashed line is a -1 power law and the green one $f_{hp,lp} = 1$.

Stokes number) and we neglect aeroelastic instabilities of the cable (as reported for instance in [19]). The forces acting to the system are shown in figure 6. For the system proposed, the equation (1) then extends to,

$$\frac{d\vec{v}}{dt} = \frac{1}{\tau_p}(\vec{u} - \vec{v}) + \frac{1}{m_p}\vec{T} + \vec{g}. \tag{6}$$

Note, that added mass has still been neglected, what requires some considerations. This term would appear on the right hand side of equation (6) as $\beta \frac{D\vec{u}}{Dt}$, where $\beta = 3\rho_f/(\rho_f + 2\rho_p)$ is a coefficient that takes into account the added mass and pressure gradient forces. It is therefore reasonable to neglect the added mass term, if $\beta a_c \ll \frac{1}{\tau_p} u_c$, where a_c and u_c are characteristic turbulence acceleration and drift velocity, respectively. Using the Heisenberg-Yaglom relation as an estimate of the characteristic acceleration ($a_c^2 = a_0 \varepsilon^{3/2} \nu^{-1/2}$ with $a_0 = \mathcal{O}(1)$), and $u_c = U_z$, this condition can be written as $\beta St \ll U_z/u_\eta$, with $u_\eta = \varepsilon^{1/4}\nu^{1/4}$ the Kolmogorov velocity of the background turbulence. This condition is satisfied in all cases, and therefore the added force term can indeed be neglected.

As maximal measured displacements of the particle do not exceed 10 cm to be compared to the total length of the wire ($L = 208$ cm), it is legitimate to assume angular oscillations to be small. Moreover, considering that turbulence fluctuations are

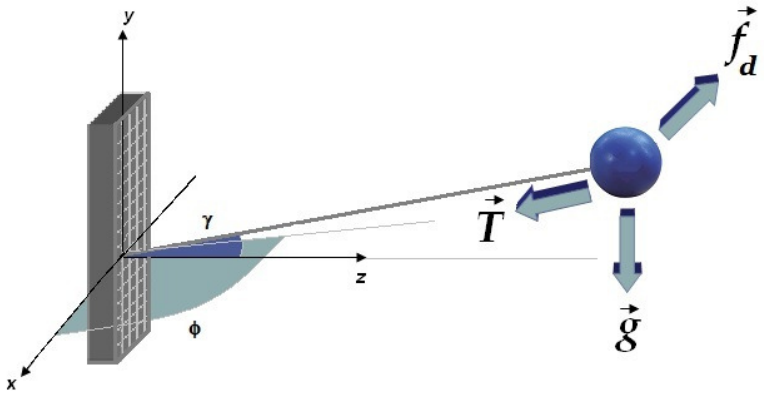

Figure 6: Forces acting in the particle: drag force, gravity and tension of the wire. γ and ϕ are the angular displacements of the wire holding the particle.

around 3%, the amplitude T of the tension will be approximated as constant. Under these assumptions, the equations of motion (6) can be be projected into the $\widehat{z}$, $\widehat{x}$ and $\widehat{y}$ coordinates, giving,

$$T = -\frac{m_p}{\tau_p} U_z, \tag{7}$$

$$\frac{dv_x}{dt} + \frac{1}{\tau_p} v_x + \frac{U_z}{\tau_p L} x = \frac{1}{\tau_p} u_x, \tag{8}$$

$$\frac{dv_y}{dt} + \frac{1}{\tau_p} v_y + \frac{U_z}{\tau_p L} y - g = \frac{1}{\tau_p} u_y. \tag{9}$$

Equations (8) and (9) in the xy plane are those of a damped oscillator forced by turbulent fields u_x and u_y.

If we now consider the Fourier transform of these equations (from now on just the x coordinate will be studied as the problem in the y axis has the same solution, adding the constant term $\vec{g}$, which gives a Dirac distribution at zero frequency in Fourier space),

we obtain the exact same form as the second order band-pass filter transfer function from equation 5, with f_0 ($\omega_0 = 2\pi f_0$) and Q given by,

$$\omega_0 = \sqrt{\frac{U_z}{L\tau_p}} \text{ and } Q = \omega_0 \tau_p = 2\pi f_0 \tau_p. \tag{10}$$

This equation is reminiscent of Tchen's filtering approach for freely advected particles except that the transfer function is now a second-order band-pass filter instead of a first-order low-pass filter (note that in the high frequency limit both are equivalent with a 20dB attenuation rate per decade). This is in qualitative agreement with the results obtained in the previous section, particularly as this model predicts the trend observed in figure 5 where f_{lp} decreases with increasing τ_p. In order to proceed to a quantitative confrontation of experiments and the model, we will rather focus in the sequel on Q and f_0 parameters which more directly parametrize the band-pass transfer function, compared to f_{lp} and f_{hp}.

Indeed, as discussed in the last section, from the 3-parameters fit of the experimental transfer function we can extract the experimental values of the filter frequency f_0 and quality factor Q. Images 7a&b show the theoretical values obtained for f_0 and Q computed using relations (10) with the actual values of U_z, L and estimates of τ_p in table 3) as a function of the experimental ones (obtained from the 3-parameters fit of measured transfer functions, as shown in figure 4). The black dashed lines represents a slope 1 line (therefore, the perfect agreement between theory and experiments). Several points can be noted. First, concerning the order of magnitude of experimental and theoretical parameters, we see that the quality factor predictions are in reasonable agreement with the experimental values. In particular, heavy particles (corresponding to points in the light green region of the plots) are predicted to have larger quality factors than light particles, in agreement with the observation that spectra in figure 4 show a clear resonant peak for the denser particles contrary to lighter particles. Regarding the natural frequency f_0, the agreement is far from being quantitatively perfect as the theoretical prediction clearly underestimates the experimental value. Nevertheless, we find that f_0^{exp} and f_0^{theo} (where the label 'exp' refers to fitted values and 'theo' to the one obtained via the model) are reasonably proportional with, $f_0^{exp} = 0.28 f_0 theo$ (orange

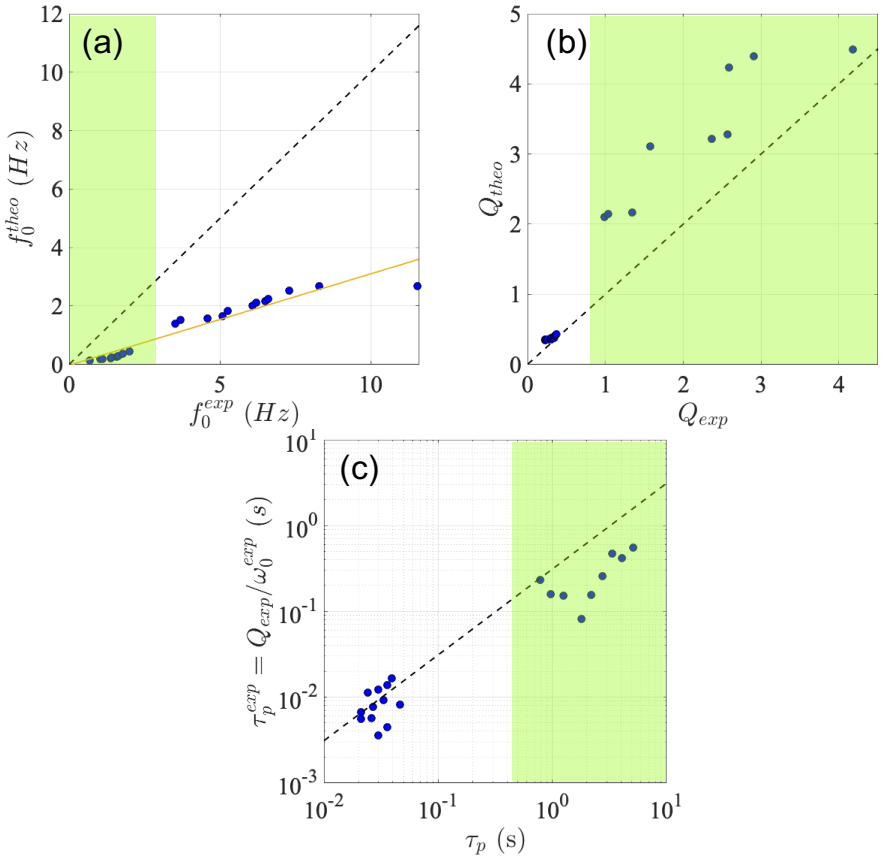

Figure 7: (a) Relation between the theoretical and the experimental values of the frequency. The blue dashed line is the proportionality relation $f_0^{theo} = f_0 exp 0.31$. (b) Relation between the theoretical and the experimental values of the quality factor. (c) Experimental particle viscous response time (defined as $\tau_p^{exp} = Q^{exp}/\omega_0^{exp}$) compared to the values from equation 2. In figures a&b, the black dashed line is the identity (with slope 1 and passing by the origin) and represents perfect agreement between theory ; in figure c it represents a linear relation between τ_p and τ_p^{exp}. In all figures the regions highlighted correspond to the three heavier particles, where the cable was not tensed and the hypotheses developed in this section are no longer valid.

solid line in figure 7a).

A possible reason for these discrepancies can be the difficulty to correctly estimate the particle response time τ_p, which is a recurrent issue in the community, in particular when finite size, finite Reynolds number effects and possibly instationary and turbulent corrections to drag coefficients are to be considered. Consequently, in figure 7c we compare the a priori estimated value of τ_p deduced from equation (2) (given in table 3), with one obtained from the band pass fit parameters on experimental data, as $\tau_p^{exp} = Q_{exp}/\omega_0^{exp}$, according to the model prediction ((10)). The figure is in logarithmic scale, due to the large range of particle viscous times explored in this work. Although no clear collapse onto a single curve is observed, points are not far from aligned onto a linear relation ($\tau_p^{exp} \approx 0.3\tau_p$), suggesting that our experimental observations and model become compatible by considering a corrected particle response time.

In the context of the band-pass filter model introduced previously, f_0 and Q appear to be the natural parameters governing particle dynamics (instead of just particle size or density for instance). Therefore we have represented the measured standard deviations of velocity (previously discussed in figure 3a) as a function of those parameters. Figure 8a shows the turbulent intensity ($\sigma_{x,y}/U_z$) of particles as a function of the experimental value of the natural frequency of the filter f_0^{exp}. In spite of some scatter it can be seen that velocity fluctuations tend to increase with f_0, while the opposite trend with Q is found (not shown here). Remembering that f_0 is a decreasing function of particle response time τ_p and Q an increasing function of τ_p (see definitions from equation 10), these trends are in qualitative agreement with the filtering prediction that fluctuations are suppressed when particle response time increases. Finally, figure 8b shows the dependency of $\sigma_{x,y}/U_z$ with the experimentally determined particle response time τ_p^{exp}, where a good collapse can be seen, and velocity fluctuations consistently decrease with increasing particles corrected response time.

To conclude this section, we assess the possible role of vortex-induced vibrations (VIV) [24, 25, 26] in the dynamics of the particles. Following van Hout *et al.* [24], we define the reduced velocity as $V_R = U_z/(f_N d_p) = S^{-1} f_S/f_N$, with S the Strouhal number of the sphere (defined as $S = f_S d_p/U_z$), f_S its vortex shedding frequency and f_N the forcing frequency. This parameter is commonly used to evaluate the importance of

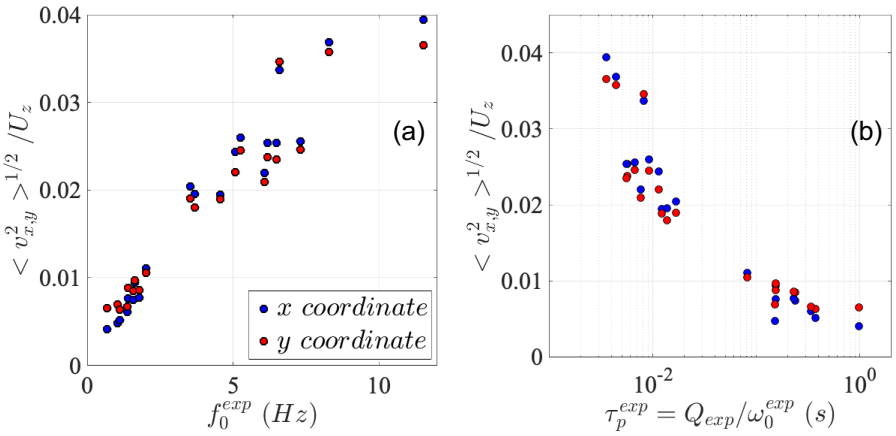

Figure 8: Fluctuations rate for both components as a function of the experimental values of f_0^{exp} (a) and τ_p^{exp} (b).

VIV effects, which are expected to lock in oscillation frequencies with vortex shedding when dominant, hence leading to resonant effects when $V_R \simeq S^{-1}$ (which would be of the order of $V_R \simeq 5$ for spheres with $S \simeq 0.2$). On the contrary, when $V_R \gg S^{-1}$ VIV effects are not considered as potentially dominant. In the present case, f_N can be taken as f_0^{theo}, f_0^{exp} or any of the peaks present in the spectra (figure 4a), which may all eventually correspond to some relevant oscillating mode of the particle dynamics.

Consistently with previous studies in similar conditions [27, 19, 14], we find that the values of V_R are too large and therefore VIV are not expected to be relevant for the experimental conditions studied in this work. Indeed, considering a Strouhal number of approximately $S = 0.2$ [28], the smallest values of $V_R S = f_S/f_N$ obtained when considering $f_N = f_0^{theo}$ and $f_N = f_0^{exp}$ are 68 and 52, respectively. Taking f_N as the frequency of the second peak observed in figure 4a (at around 5Hz, that correspond to sphere 7), gives a value of $V_R \simeq 300$. We therefore find that the shedding frequency of the system is always significantly larger than the natural frequencies observed in our system, what indicates that the fluctuating dynamics is not primarily governed by VIV effects.

5. Conclusions

This work focus on the fundamental features of particle / turbulence interactions, with the particular goal to emphasize filtering effects due to particle's inertia by considering the situation of a particle with strong relative slippage velocity compared to the turbulent fluctuations.This has been accomplished by considering a semi-constrained particle dynamics, where a dominant drag is imposed by a strong particle-fluid drift velocity. At the same time, this arrangement is particularly interesting as it is analog to a propelled system and different towing configurations.

The analysis of towed particles dynamics shows a clear trend of fluctuations (both for velocity and acceleration) to be reduced with increasing particle inertia, with a loss of Lagrangian intermittency (acceleration fluctuations becoming Gaussian, contrary to what has been reported for finite size freely advected inertial particles).

While we do see an effect of τ_p in the cross-stream components of the velocity and the acceleration, in our configuration the parameter not affected by τ_p is drift, as it is controlled mainly by the freestream velocity. Nevertheless, the coupling of the particle with the turbulent flow is affected by τ_p, but not in the same way as it occurs for freely advected particles. The large drift in this system adds a crossing-trajectories effect, that is ultimately responsible for the Gaussianization of the acceleration. This effect is usually not observed for small freely advected particles in turbulence, but may eventually become relevant, for instance, for heavily settling particles (as rain droplets) with important relative drift velocity prone to promote similar crossing trajectories effects. Our results therefore contribute to the modelling of freely-advected particles in such conditions as they allow to explore a simplified system where the slippage velocity has been artificially increased.

The spectral signature of particles dynamics is found to be well described by a filtering mechanism with transfer functions of particles properly fitted by a second-order band-pass filter acting on the carrier velocity field power spectral density. Furthermore, based on first principles considerations, a simple model has been found to correctly predict such dynamics, where the coupling between particle and turbulence is primarily driven by the drag force.

The proposed model for particles dynamics works reasonably well, as it qualitatively retrieves the band-pass filter scenario, and becomes quantitatively accurate when a corrected particle response time is adjusted. In particular, the model captures the main features of the fluid-particle transfer function, explaining for instance the presence (or absence) of resonant peaks in the particles dynamics spectra (characterized by the quality factor of the band-pass transfer function) depending on particles properties. The natural frequency of the transfer function is not compatible with the *a priori* estimated particle response time, based on classical drag coefficient parametrisations. The experimentally determined natural frequency, obtained by fitting the experimental transfer function with the band-pass filter model, allows however to determine a corrected experimental particle response time. Reasons for this correction remain unclear and might be related to non-stationary effects or to the influence of background turbulence on the spheres effective drag coefficient.

Finally this work raises important conclusions in terms of the issue of turbulent transport of finite size inertial particles. As mentioned in the Introduction, when considering the problem of particles freely advected by a turbulent flow, classical models usually consider the drag force as leading one acting on the particles, as equation (1). The present work shows that this assumption must be carefully considered. Indeed even in a case as the one investigated here, which has been tailored to impose the leading role to drag, agreement with experimental observations remains essentially qualitative, and subtle corrections still appear to be more necessary to reach a quantitative agreement. On the other hand, these observations point to the possible relevance of using such minimal drag models for finite size inertial particles with important relative drift, on the condition that an appropriate corrected particle response time is used.

References

[1] M. R. Maxey, J. J. Riley, Equation of motion for a small rigid sphere in a nonuniform flow, Physics of Fluids 26 (1983) 883.
URL `http://link.aip.org/link/?PFLDAS/26/883/1`

[2] R. Gatignol, The faxen formulae for a rigid particle in an unsteady non-uniform stokes flow, J. Mec. Theor. Appl 1 (2) (1983) 143–160.

[3] C. Crowe, J. D. Schwaezkopf, M. Sommerfeld, Y. Tsuji, Multiphase Flows with droplets and particles, second edition Edition, CRC Press, 2012.

[4] E. Calzavarini, R. Volk, M. Bourgoin, E. Lévêque, J.-F. Pinton, F. Toschi, et al., Acceleration statistics of finite-sized particles in turbulent flow: the role of faxén forces, Journal of Fluid Mechanics 630 (2009) 179.
URL http://journals.cambridge.org/production/action/cjoGetFulltext?fulltextid=5876816

[5] M. Bourgoin, H. Xu, Focus on dynamics of particles in turbulence, New Journal of Physics 16 (8) (2014) 085010.

[6] J. Hinze, Turbulence, 2nd ed. (New York, 1975)., 2nd Edition, McGraw-Hill, New york, 1975.

[7] J. Bec, L. Biferale, G. Boffetta, A. Celani, M. Cencini, A. Lanotte, S. Musacchio, F. Toschi, Acceleration statistics of heavy particles in turbulence, Journal of Fluid Mechanics 550 (349) (2006) 10.
URL http://journals.cambridge.org/production/action/cjoGetFulltext?fulltextid=409552

[8] S. Ayyalasomayajula, A. Gylfason, L. R. Collins, E. Bodenschatz, Z. Warhaft, Lagrangian measurements of inertial particle accelerations in grid generated wind tunnel turbulence, Physical Review Letters 97 (14) (2006) 144507.

[9] V. Mathai, E. Calzavarini, J. Brons, C. Sun, D. Lohse, Microbubbles and microparticles are not faithful tracers of turbulent acceleration, Physical review letters 117 (2) (2016) 024501.

[10] G. T. Csanady, Turbulent Diffusion of Heavy Particles in the Atmosphere, Journal of the Atmospheric Sciences 20 (1963) 201–208. doi:10.1175/1520-0469(1963)020<0201:TDOHPI>2.0.CO;2.

[11] H. L. Grant, R. W. Stewart, A. Moilliet, Turbulence spectra from a tidal channel, Journal of Fluid Mechanics 12 (2) (1962) 241–268. doi:10.1017/S002211206200018X.

[12] J. S. Jaffe, P. J. Franks, P. L. Roberts, D. Mirza, C. Schurgers, R. Kastner, A. Boch, A swarm of autonomous miniature underwater robot drifters for exploring submesoscale ocean dynamics, Nature Communications 8 (2017) 14189. doi:10.1038/ncomms14189.

[13] E. Calzavarini, Y. X. Huang, F. G. Schmitt, L. P. Wang, Propelled microprobes in turbulence, Physical Review Fluids 3 (5) (2018) 1–13. arXiv:1802.00189, doi:10.1103/PhysRevFluids.3.054604.

[14] M. Obligado, C. Baudet, Y. Gagne, M. Bourgoin, Constrained dynamics of an inertial particle in a turbulent flow, in: Journal of Physics: Conference Series, Vol. 318, IOP Publishing, 2011, p. 052016.

[15] F. Cichos, K. Gustavsson, B. Mehlig, G. Volpe, Machine learning for active matter, Nature Machine Intelligence 2 (2) (2020) 94–103.

[16] M. Bourgoin, R. Kervil, C. Cottin-Bizonne, F. Raynal, R. Volk, C. Ybert, Kolmogorovian active turbulence of a sparse assembly of interacting marangoni surfers, Physical Review X 10 (2) (2020) 021065.

[17] S. Colabrese, K. Gustavsson, A. Celani, L. Biferale, Smart inertial particles, Physical Review Fluids 3 (8) (2018) 084301.

[18] N. Mazellier, Dynamique spatio-temporelle du champ de vorticité en turbulence, Ph.D. thesis, Université Joseph Fourier (2005).

[19] M. Obligado, M. Bourgoin, An experimental investigation of the equilibrium and stability of long towed cable systems, New Journal of Physics 15 (4) (2013) 043019.
URL http://iopscience.iop.org/1367-2630/15/4/043019

[20] P. P. Brown, D. F. Lawler, Sphere drag and settling velocity revisited, Journal of environmental engineering 129 (3) (2003) 222–231.

[21] N. M. Qureshi, U. Arrieta, C. Baudet, A. Cartellier, Y. Gagne, M. Bourgoin, Acceleration statistics of inertial particles in turbulent flow, The European Physical Journal B 66 (4) (2008) 531–536.
URL http://link.springer.com/article/10.1140/epjb/e2008-00460-x

[22] R. Zimmermann, Y. Gasteuil, M. Bourgoin, R. Volk, A. Pumir, J.-F. Pinton, Rotational intermittency and turbulence induced lift experienced by large particles in a turbulent flow, Physical review letters 106 (15) (2011) 154501.
URL http://link.aps.org/doi/10.1103/PhysRevLett.106.154501

[23] C.-M. Tchen, Mean value and correlation problems connected with the motion of small particles suspended in a turbulent fluid, Ph.D. thesis, TUDelft (1947).
URL http://www.narcis.nl/publication/RecordID/oai:tudelft.nl:uuid:65d1454c-e070-44f3-a28a-9c03cc9868ef

[24] R. van Hout, A. Krakovich, O. Gottlieb, Time resolved measurements of vortex-induced vibrations of a tethered sphere in uniform flow, Physics of Fluids 22 (8) (2010) 087101.

[25] L. Eshbal, D. Kovalev, V. Rinsky, D. Greenblatt, R. van Hout, Tomo-piv measurements in the wake of a tethered sphere undergoing viv, Journal of Fluids and Structures 89 (2019) 132–141.

[26] R. Govardhan, C. Williamson, Vortex-induced vibrations of a sphere, Journal of Fluid Mechanics 531 (2005) 11–47.

[27] M. Obligado, N. Machicoane, A. Chouippe, R. Volk, M. Uhlmann, M. Bourgoin, Path instability on a sphere towed at constant speed, Journal of Fluids and Structures 58 (2015) 99–108.

[28] E. Achenbach, Vortex shedding from spheres, Journal of Fluid Mechanics 62 (2) (1974) 209–221.